IRAQI JOURNAL OF APPLIED PHYSICS
Vol. 22, No. 2, April-June 2026, pp. 159-170

Thermodynamic Study of Heavy Metal Removal from Aqueous Solutions Using a Sustainable Source

Sofian H. Hussen [1]
Wahran M. Saod [2*]

[1] Department of Chemistry, College of Education for Pure Sciences, University of Anbar, Ramadi, IRAQ
[2] Department of Chemistry, College of Science, University of Anbar, Ramadi, IRAQ
* Corresponding author email: sc.wahran.s@uoanbar.edu.iq

Researchers are increasingly studying the extraction of mesoporous silica ($mSiO_2$) from natural sources as a sustainable and low-cost source in response to the growing demand for environmentally friendly materials worldwide. Because of their high silicon dioxide (SiO_2) content, natural rocks like diatomite, volcanic tuff, porcelanite, and kaolinitic clay are promising raw materials for the synthesis of mesoporous silica. Mesoporous silica is distinguished by its high surface area, tunable pore architecture, and ordered porous structure with pore diameters ranging from 2 to 50 nanometers. Even at low concentrations, recent research has demonstrated the high adsorption efficiency of $mSiO_2$, particularly the modified variants, in eliminating hazardous heavy metal ions like Pb^{2+}, Cd^{2+}, and Cr^{3+}. Under various circumstances, we evaluated the synthesized silica's capacity to remove the ions Pb^{2+}, Cd^{2+}, and Cr^{3+} from water samples. Including pH, initial concentration, and contact time, the most effective removal rates. The optimum conditions for removal of them over 97.8% of Pb^{2+}, 98% of Cd^{2+}, and 99.6% of Cr^{3+} ions. At pH = 8 and a contact time of 90 minutes, the best contact time for removal was 90, the optimum concentration was 30, the optimum mass was 0.02, and the temperature was 298 K at a temperature of 298 K. We examined the adsorption and utilized the Freundlich, Langmuir, and Temkin isotherm models to analyze the absorption data.

Keyword: Thermodynamics; Mesoporous silica; Porcelain rock; Isotherms
Received: 8 June 2025; Revised: 18 August 2025; Accepted: 25 August 2025

1. Introduction

Researchers are increasingly looking to extract mesoporous silica ($mSiO_2$) from natural sources as sustainable and affordable substitutes for industrial products in response to the growing demand for environmentally friendly nanomaterials worldwide. Because of their high silicon dioxide (SiO_2) content, natural rocks like diatomite, volcanic tuff, porcelanite, and kaolinitic clay are promising raw materials for the synthesis of mesoporous silica [1]. Economically speaking, the viability of $mSiO_2$ production is increased by the use of plentiful and inexpensive sources such as fly ash, porcelanite, and kaolin, which supports local resource utilization in environmental applications and circular economy strategies [2]. Mesoporous silica has several unique properties that make it a promising material for environmental and industrial applications, particularly in the removal of pollutants from water. Its most notable advantages include its high surface area, uniform pore distribution, and ease of chemical surface modification to suit various types of pollutants. It also has good thermal and chemical stability, giving it the ability to withstand harsh operating conditions. Furthermore, its ability to be formed into various nanoscale sizes and shapes increases its efficiency in surface interactions and adsorption. These properties make mesoporous silica an effective and versatile platform for water High surface area, adaptable pore architecture, and a well-organized porous structure with pore diameters between 2 and 50 nanometers are characteristics of mesoporous silica [3,4]. Furthermore, because organic or inorganic functional groups can readily alter its surface chemistry, it is highly versatile for a range of environmental applications [5] particularly in adsorption-based water purification systems. Even at low concentrations, recent studies have shown that m SiO_2, it is a high adsorption effectiveness in removing dangerous heavy metal ions like lead (Pb^{2+}), cadmium (Cd^{2+}), and Trichromium (Cr^{3+}) [6]. Because these ions are persistent in aquatic environments and bioaccumulative, they pose significant risks to human health and the environment. Therefore, compared to other treatment techniques like ion exchange, chemical precipitation, membrane filtration, reverse osmosis, and oxidation-reduction, adsorption stands out as being easier, less expensive, and more efficient [7]. Surface modification is necessary to increase mesoporous silica's adsorption capacity. Uptake performance has been greatly enhanced by functional components such as amines and thiols (-SH), which have shown selectivity towards particular metal ions. Some reports have shown capacities exceeding 200 mg/g for Pb^{2+} ions [9,10]. The adsorption processes, which are impacted by variables like solution pH, temperature, and surface functionalization, generally include physical adsorption, ion exchange, and surface complexation [11]. Furthermore, mesoporous silica's chemical and structural stability make it suitable for long-term industrial deployment by enabling repeated use through straightforward regeneration procedures. Understanding the nature and capacity of the

adsorption process is further aided by the use of adsorption isotherm models like Langmuir and Freundlich, which offer information on whether interactions are monolayer or multilayerand whether they are homogeneous or heterogeneous [12]. Aquatic contamination is largely caused by the growing release of heavy metals from industries like tanning, mining, battery manufacturing, refinery, and the manufacture of paints, dyes, and pesticides [13,14]. Furthermore, increased concentrations of these metals in water bodies are caused by natural processes like erosion, spring water leaching, volcanic activity, and microbial activity [15]. Even though trace levels of heavy metals are necessary for some biological processes, an excessive buildup can have serious negative health effects, such as neurological damage, nephrotoxicity, and cancer [16]. In light of this, research is now focused on creating adsorbents that are both highly effective and eco-friendly. Mesoporous silica from natural sources is one of the most promising options due to its unique physicochemical properties, ease of functionalization, and affordability. Thus, the goal of the current study is to determine how well mesoporous silica removes toxic metal ions from aqueous solutions and investigate how it is produced from locally accessible, naturally occurring rocks. In order to develop a sustainable strategy for heavy metal remediation, the study also investigates theoretical adsorption models, underlying mechanisms, and operational parameters that impact adsorption [17].

2. Materials and Methodology

A primary pathway for the synthesis of mesoporous silica ($mSiO_2$) was adopted: the natural method to ensure safety. Porcelainite rocks were used as a natural raw source of silica, obtained from the Geology Department of the College of Science at the University of Anbar. Its chemical composition can vary depending on the protolith and formation conditions, but it generally has high silica (SiO_2) and alumina (Al_2O_3) content, resembling porcelain. Silica-rich porcelainite (closer to chert/flint): >85% SiO_2, low Al_2O_3. Argillaceous porcelainite (clay-derived): higher Al_2O_3 (10-20%), moderate SiO_2 (60-80%). The extraction process also involved the use of several chemical auxiliaries in the purification and extraction steps, such as lead, cadmium, and chromium nitrates, in addition to strong bases and acids such as hydroxide, sodium, sulfuric acid, and hydrochloric acid. This methodology represents an integrated approach that combines industrial and natural sources to produce $mSiO_2$, taking into account efficiency, cost, and environmental feasibility.

To get rid of surface contaminants, the natural porcelainite rocks were first thoroughly cleaned with distilled water. To guarantee moisture removal, the samples were cleaned and then oven-dried for an entire night at 90°C. After that, they were hand-ground and sieved through a 180-µm sieve to produce a fine, uniform powder. To increase the powder's reactivity, it was thermally activated for three hours at 500°C. A 150 ml of a 3 mol/L sodium hydroxide (NaOH) solution was added to 2.5 g of the activated sample in a 250 ml round-bottom flask with a reflux condenser in order to extract the silica. To change the insoluble silica into soluble sodium silicate, this mixture was continuously agitated for 24 hours at 300 rpm. The selection of a stirring speed of 300 rpm for the extraction process appears to be based on standard practices and previous studies, as good silica was obtained without material effects, and was not specifically optimized for this study. This speed is commonly used in similar synthesis procedures to ensure adequate dispersion of the reactants, prevent precipitation, and promote uniform reaction conditions. Future studies could explore a range of stirring speeds to evaluate their effect on silica yield, surface area, pore structure, and adsorption performance, potentially contributing to improved process efficiency and material properties. Ash-free filter paper was used to filter the resultant mixture (Whatman no. 41) and washed with hot water that had been distilled. Using 5 mol/L sulfuric acid (H_2SO_4) and vigorous stirring, the pH of the clear solution was first lowered to less than 10 before being gradually raised to 7 to start the silica precipitation process. After completing this step, a soft, white silica gel was produced, which was allowed to fully mature for 24 hours at room temperature. The gel was filtered, rinsed with distilled water to get rid of any remaining sulfate ions, and then dried for 24 hours at 80°C and 110°C. A fine, white, mesoporous silica powder that is suitable for environmental applications was finally produced by calcining the dried product for two hours at 800°C [18,19].

In order to determine the adsorption capacity of $mSiO_2$ to adsorb Pb^{2+}, Cd^{2+}, and Cr^{3+} ions at different concentrations (10, 20, 30, 40, and 50 mg/L), we carried out a batch adsorption study with pH adjustment (pH = 8) and a contact duration of two hours at 25°C. 30 mL centrifuge tubes were used for the experiments. The tubes were filled with 10 mL of solutions containing different concentrations of Pb^{2+}, Cd^{2+}, and Cr^{+3} ions. To get rid of any leftover suspended material, the samples were centrifuged for ten minutes at 5000 rpm. To guarantee the best possible interaction between the adsorbent and adsorbate, the samples were first shaken in a water bath at a speed of 100 rpm. Using the corresponding equations (1) and (2), we determined the equilibrium adsorption capacity (q_e mg/g) and the percentage removal effectiveness (%R) [20]

$$\%R = 100 \times \frac{C_0 - C_e}{C_0} \quad (1)$$

$$q_e = \frac{(C_0 - C_e)V}{m} \quad (2)$$

where C_e is the equilibrium metal ion concentration, m is the adsorbent's mass (g), V is the solution's volume (L), and C_0 stands for the starting metal ion

3. Results and Discussion

Fourier-transform infrared (FTIR) spectroscopy is frequently used to compare structural characteristics between compounds and identify functional groups in both pure substances and composite materials. The method is based on atoms' and molecules' vibrational movements, which correlate to particular infrared absorption frequencies ($mSiO_2$) has strong absorption bands in the 1400-1700 and 800-1000 cm^{-1} regions of its FTIR spectrum. The FTIR spectrum shown in Fig. (1) indicates the presence of distinct functional groups in the sample. The first band (1400-1700 cm^{-1}) is attributed to the vibrations of carbonyl bonds (C=O) in ketones or esters (around 1700 cm^{-1}) and double bond vibrations (C=C) in aromatic rings (1600 cm^{-1}), in addition to the possible presence of N=O bonds or O-H bond distortions. The second band (800-1000 cm^{-1}) mainly refers to the vibrations of the Si-O-Si bonds characteristic of silicon materials, typically appearing at around 1000 cm^{-1}, with the possibility of silicon-carbon (Si-C) bonds at shorter wavelengths. The Si–O stretching vibrations commonly found in silicate materials and mesoporous silica frameworks are responsible for a particularly strong peak that emerges around 1000 cm^{-1}. All FTIR results show that the sample contains a mixture of organic and inorganic functional groups, with Si-O-Si bonds clearly predominating, as peaks in the 1000-1200 cm^{-1} range are the most intense. Other peaks indicate the presence of organic impurities or traces of solvents or moisture of the examined samples also exhibit a distinctive band at about 790 cm^{-1}, which corresponds to the symmetric stretching of Si–O–Si linkages and is suggestive of the silica network structure [22] as shown in Fig. (1).

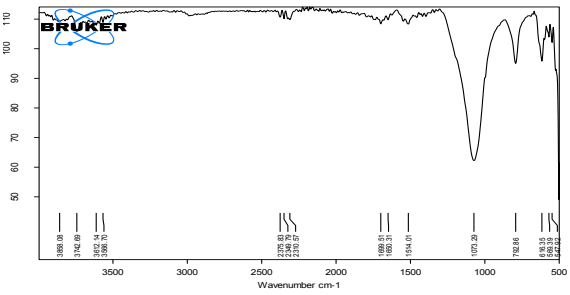

Fig. (1) FTIR spectra of $mSiO_2$ by natural source

An X-ray diffraction (XRD) pattern of a mesoporous silica ($mSiO_2$) sample is shown in Fig. (2). The distribution of crystalline phases in the sample is depicted in the pattern. Amorphous materials like silica are characterized by broad, non-sharp diffraction peaks, especially at $2\theta \approx 22°$. The values of the 2θ in the pattern are 25.2° and 27.8°, corresponding to Al_2Fe anorthic, according to JCPDS card 00-033-0019. At 2θ=43.2° and 56.2°, they correspond to $Al_2Si_4O_{10}$ anorthic, according to JCPDS card 00-025-0021. At 2θ=77.2°, they correspond to Fe_2O_3 hexagonal, corresponding to JCPDS card 01-076-1821. This suggests that the sample's predominant structure is amorphous. A few weak secondary peaks also show up at different angles (e.g., 102, 110, 202, etc.), which could be the result of natural impurities in the raw material or crystalline impurities from undissolved residues. These findings verify the sample's high proportion of amorphous silica, a composition that is generally preferred in environmental applications like pollutant removal because of its high porosity and active surface as shown in Fig. (2).

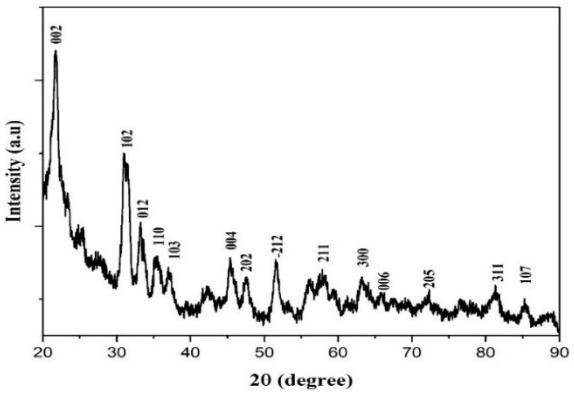

Fig. (2) XRD pattern of $mSiO_2$ by natural source

Using energy-dispersive X-ray spectroscopy (EDX), the elemental makeup and purity of the synthesized mesoporous silica ($mSiO_2$) material. This analysis is critical for confirming the absence of unwanted metallic or organic impurities and for verifying the integrity of the silica framework. Mesoporous silica is an inorganic material composed primarily of silicon and oxygen. It is characterized by a regular lattice structure with fine pores, as in well-known structures such as $mSiO_2$) and SBA-15. The EDX results of the prepared mesoporous silica sample revealed two distinct peaks: one at an energy of approximately 1.74 keV, attributed to the Kα emission line of silicon, while the second peak appeared at approximately 0.52 keV, representing the Kα line of oxygen. These peaks confirm that the sample is composed mainly of Si and O, materials and does not significantly affect the purity of the extracted silica contamination from extraneous elements. Notably, the sample was later used as an adsorbent for heavy metal ions such as Pb^{2+}, Cd^{2+},and Cr^{+3} for which EDX analysis can also be applied to confirm metal loading following the adsorption process [24] as shown in table (1) and Fig. (3).

Field-emission scanning electron microscopy (FE-SEM) was used to analyze the surface morphology and microstructural properties of mesoporous silica ($mSiO_2$) as shown in Fig. (4). The FE-SEM images show that the $mSiO_2$ has a uniform surface made up of densely grouped quasi-spherical particles. This morphological characteristic is typical of controlled-

environment mesoporous silica materials and aligns with previously documented structural properties of materials of the $mSiO_2$ type. The high surface energy of the fine particles, which encourages clustering during the drying or calcination stages, could be the cause of the observed particle aggregation [25].

Table (1) Elemental analysis of $mSiO_2$

Element	Atomic %	Atomic % Error	Weight %	Weight % Error
C	11.7	0.5	7.5	0.3
O	59.9	0.4	51.1	0.4
Na	5.9	0.1	7.2	0.1
Si	20.2	0.1	30.3	0.1
S	2.3	0.0	3.9	0.1

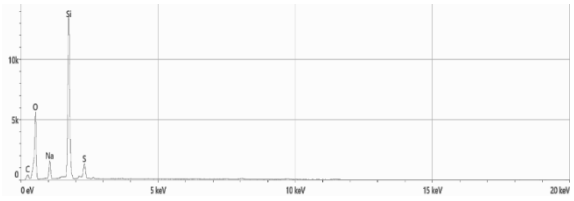

Fig. (3) EDX analysis of the mesoporous silica

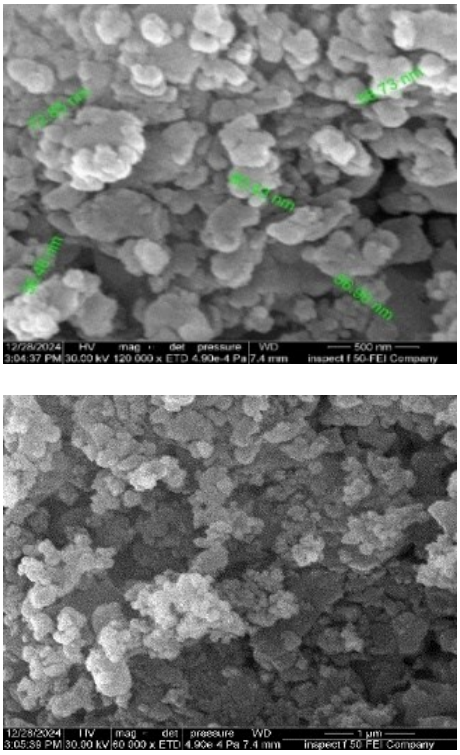

Fig. (4) FE-SEM images of $mSiO_2$ by natural source

Transmission electron microscope (TEM) images show the nanostructure of the extracted mesoporous silica sample, revealing the regular arrangement of nanoscale pores, reflecting the characteristic structure of $mSiO_2$ or SBA-15 materials. The images show a regular cylindrical shape of the pores, aligned in parallel, indicating a hexagonal or pseudo-regular network structure, a characteristic feature of mesoporous silica prepared by templated synthesis. The pore diameters seen in the images range from 2 to 10 nm, placing the material within the IUPAC classification of mesoporous silica. The particles also exhibit good dispersion and a regular porous structure without agglomerations or distortions, indicating the quality of the preparation and the stability of the material. This structural arrangement enhances the specific surface area of the material and provides a large number of active sites for adsorption, making it effective in applications for removing contaminants such as heavy metal ions from aqueous solutions. The presence of this organized structure is an important indicator of the success of the preparation and control of synthetic conditions such as temperature, reagent ratio, and reaction time as shown in Fig. (5) [26].

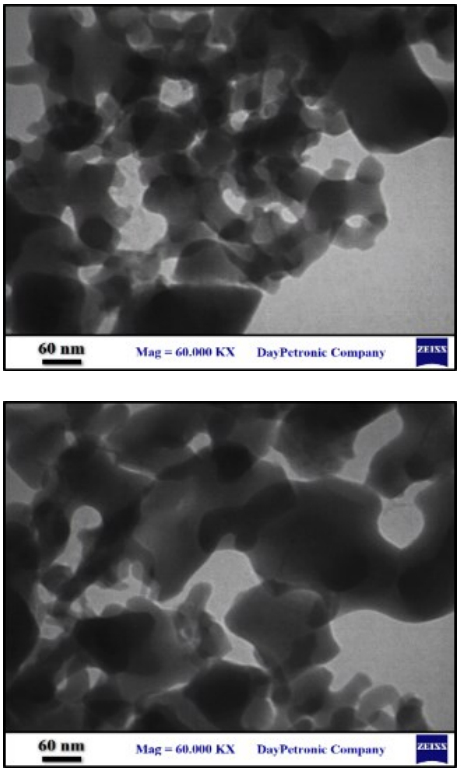

Fig. (5) TEM images of $mSiO_2$ by natural source

When characterizing solid materials especially those that come from natural geological sources, engineered adsorbents, or chemically modified composites surface area measurement is a crucial parameter. The Brunauer–Emmett–Teller (BET) analysis of a mesoporous silica ($mSiO_2$) sample is displayed in the attached figures. A traditional linear BET curve between 1 and 2 is depicted in the first figure. The validity of the BET model and the dependability of the generated data are demonstrated by this curve's obvious linearity (P_0/P), which falls within the suggested range of 0.05-0.20. Based on the

vertical section and this line's slope, it is possible to compute specific surface area (SSA), which indicates how much the sample's porous structure has developed. The adsorption/desorption isotherm curve is displayed in the second figure for the entire range of relative pressures (0-1). This curve exhibits typical IUPAC type IV behavior, which is defined by a broad "hysteresis loop" at high relative pressure. This pattern is typical of mesoporous materials like $mSiO_2$ or SBA-15 and indicates the presence of cylindrical or narrow-necked pores. The resulting pore sizes are primarily between 2 and 50 nm, which suggests that the pores have a high capacity to hold molecules, which is consistent with mesoporous silica's characteristics. According to these findings, the prepared material is very effective in adsorption applications, especially the removal of heavy metal ions from aqueous solutions, because it has a highly porous surface with a uniform pore size distribution. These findings demonstrate that the prepared silica is appropriate for use in environmental remediation applications and that its exceptional physical characteristics enhance adsorption efficiency by expanding the material-solution contact area [27].

$$\left(\frac{P}{P_0}\right).\left[\frac{(C-1)}{(V_m \cdot C)}\right]+\frac{1}{(V_m \cdot C)}=\frac{P}{[V(P_0-P)]} \qquad (3)$$

V is the volume of gas adsorbed at an equilibrium pressure P, V_m is the monolayer adsorbed gas volume, P_0 is the saturation pressure of the adsorbate gas at the experimental temperature, C is a dimensionless constant that is related to the heat of adsorption of the first layer compared to the heat of liquefaction of the adsorbate gas as shown in table (2) and Fig. (6)

Table (2) Surface area and pore volume data obtained for $mSiO_2$ (BET and NLDFT model calculated)

Nitrogen	S_{BET}, m^2/g	Pore volume, cc/g
$mSiO_2$	12.5323	0.023909

To introduce the nitrogen adsorption-desorption, the N_2 sorption isotherms (Fig. 6) show a noticeable nitrogen uptake at a low relative pressure ($P/P_0<0.1$), which is indicative of a high surface area for this sample, and which is followed by the second step in the N_2 uptake with the relative pressure of ~0.3, which is due to the nitrogen multi-layer adsorption in the mesopores of the $mSiO_2$ type material. The data analysis for $mSiO_2$ shows a narrow pore size distribution peaking at 3.2 nm, with the pore volume of 0.503 cm^3/g and the surface area of 601 m^2/g (table 1), which is typical of mesoporous silicas, such as $mSiO_2$. The data analysis for yields the pore volume of 0.115 cm^3/g and surface area of 138 m2/g [28,29] as shown in Fig. (6).

4. Study of Factors Affecting Removal

One of the most crucial factors influencing an adsorbent's adsorption behavior is its pH, which has a direct impact on the adsorbent's surface charge as well as the chemical makeup of metal ions like (Pb^{2+}, Cd^{2+}, and Cr^{3+}) in aqueous media. In order to identify the ideal pH range for the efficient removal of these ions, the impact of pH on the adsorption efficiency of mesoporous silica ($mSiO_2$) was assessed in this work.

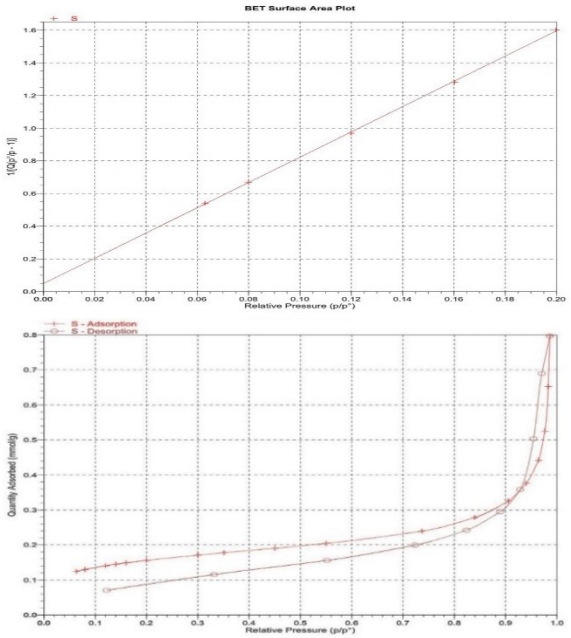

Fig. (6) The pore size distribution and the nitrogen adsorption-desorption isotherm for $mSiO_2$

Adsorption tests were carried out with 0.01 g of $mSiO_2$, an initial metal ion concentration of 100 mg/L [30], and a contact time of two hours at a constant temperature of 25°C. Each solution's pH was meticulously adjusted to precise levels in order to investigate its impact on removal performance (2, 3, 4, 5, 6, 7, and 8). The ideal pH range was discovered to be pH=8. The adsorption behavior of mesoporous silica ($mSiO_2$) is strongly influenced by pH due to changes in surface charge. The point of zero charge (PZC) for silica typically lies around pH 2-3. Below the PZC, the surface is positively charged, leading to electrostatic repulsion of cationic metal ions (e.g., Pb^{2+}, Cd^{2+}, Cr^{3+}). As pH increases beyond the PZC, surface silanol groups (Si–OH) deprotonate, generating negatively charged sites ($Si–O^-$. At pH≈8, the silica surface becomes highly negative, which enhances the electrostatic attraction and surface complexation with metal cations. This results in maximum adsorption efficiency, as observed experimentally. Thus, pH of 8 offers optimal conditions for metal ion uptake via strong ion–surface interactions The most appropriate environment for adsorption on the surface of porous silica extracted from natural rocks was then determined by calculating the percentage of removal of Pb^{2+}, Cd^{2+}, Cr^{3+} under each pH condition, as illustrated in table (2) and Fig. (7) [31]

$$q_e=\frac{(C_O-C_e)\times V_{(L)}}{m_{(mg)}} \qquad (4)$$

The variables included in this equation are the initial concentration C_0 (mg/L), C_e is the equilibrium metal ion concentration (mg/g), V is the solution's volume (L), and m is the adsorbent's mass (g)

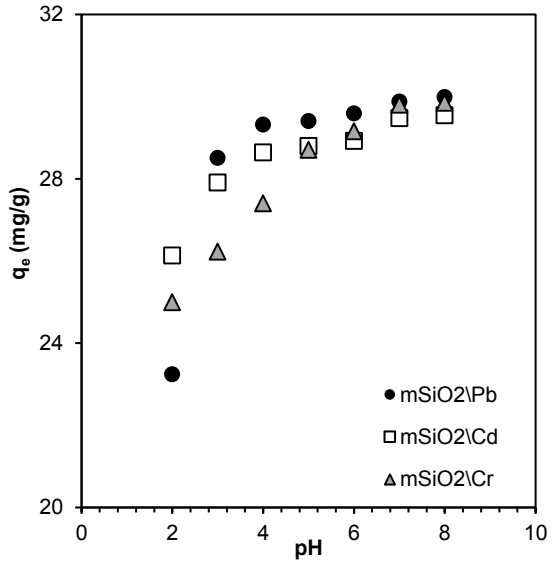

Fig. (7) The impact of pH on the capacity of Pb^{2+}, Cd^{2+}, Cr^{3+} ions using mesoporous silica ($mSiO_2$)

Determining the optimal time frame is essential to optimizing adsorption efficiency, as contact time is a critical factor influencing heavy metal ion adsorption behavior. Evaluating the effect of contact duration aids in determining the equilibrium time required to efficiently remove metal ions and improves comprehension of the adsorption dynamics. For all adsorbents, increasing the contact time generally improves adsorption efficiency up until equilibrium is reached, after which there is no discernible change in removal [32]. The effective removal percentage of Pb^{2+}, Cd^{2+}, and Cr^{3+} ions in this study was determined under carefully monitored conditions: solution pH was kept at 8, the temperature was set at 25°C, the initial metal ion concentration was 100 mg/L, and the adsorbent dosage was 0.02 g as indicated in table (3), adsorption was tracked over a range of contact times (10, 20, 30, 45, 60, 90, and 120 minutes). Each ion's equilibrium point and adsorption rate were evaluated using the data gathered. The process by which Pb^{2+}, Cd^{2+}, and Cr^{3+} ions adsorb onto mesoporous silica ($mSiO_2$) presents a rapid uptake during the first 10 minutes, followed by a gradual slowdown until equilibrium is reached, as illustrated in the corresponding figure. The saturation of accessible active sites on the surface is indicated by the adsorption rate becoming almost independent of contact time beyond this point of the adsorbent. This behavior can be explained by the abundance of unoccupied adsorption sites and the large specific surface area of $mSiO_2$ at the beginning of the process. During the first rapid phase of adsorption, which is primarily regulated by surface diffusion, metal ions interact quickly with the external surface of the silica particles. Intra-pore diffusion, in which ions move into the material's inner porous structure, takes over as the adsorption rate decreases [33]. According to the experimental findings, the optimal contact time for Pb^{2+}, Cd^{2+}, and Cr^{3+} ions was found to be 60 minutes under the following conditions: pH = 8, initial concentration of 100 mg/L, and temperature of 25°C as shown in table (3) and Fig. (8).

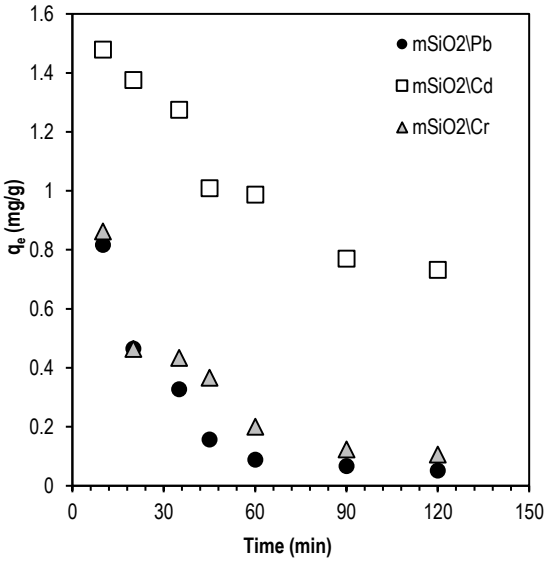

Fig. (8) Impact of contact time the capacity of (Pb^{2+}, Cd^{2+} and Cr^{3+}) ions using mesoporous silica ($mSiO_2$)

The impact of initial metal ion concentration on the adsorption efficiency of mesoporous silica ($mSiO_2$) was examined in order to evaluate the removal of Pb^{2+}, Cd^{2+}, and Cr^{3+} ions. Experiments were conducted with a fixed dosage of 0.01 g of adsorbent at pH 8 and 25°C. The findings, which are summed up in the relevant tables, indicate that as the initial concentration of metal ions increases, the removal efficiency falls. This decline can be explained by the fact that there are fewer adsorption sites on the surface of $mSiO_2$ relative to the increasing number of metal ions in solution. On the other hand, because the adsorbent surface could absorb more ions at higher ion concentrations, the adsorption capacity (q_e) showed an increasing trend. This inverse connection between removal effectiveness and adsorption capacity agrees with earlier results [27,28]. The initial concentration was determined to be 10 mg/L based on the data. At 25°C and pH 8, it produced the highest removal efficiency for all three ions (Pb^{2+}, Cd^{2+}, and Cr^{3+}), while at higher concentrations, like 50 mg/L, the adsorption capacity was optimized as shown in table (4) and Fig. (9).

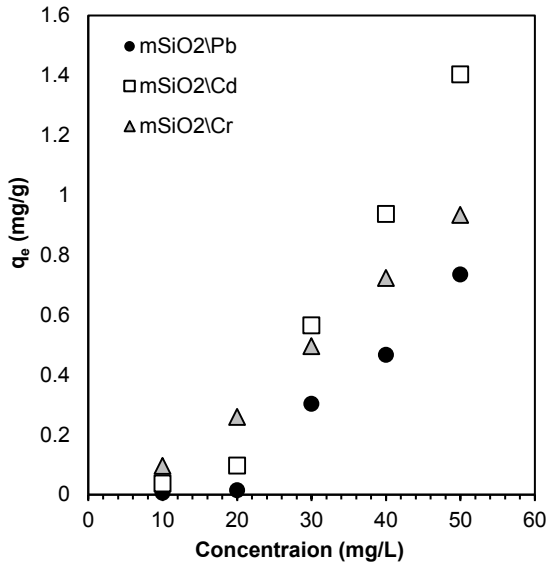

Fig. (9) Effect of the initial concentration on the capacity of Pb^{2+}, Cd^{2+} and Cr^{3+} ions using mesoporous silica ($mSiO_2$)

4.4 Effect Adsorbent mass

To find the ideal adsorbent mass for maximum removal efficiency, the effects of various mesoporous silica ($mSiO_2$) dosages on the adsorption of Pb^{2+}, Cd^{2+}, and Cr^{3+} ions were examined. Dosages of 0.05 g, 0.01 g, 0.02 g, 0.03 g, and 0.04 g were tested. Adsorption tests were conducted with a solution pH of 8, a constant temperature of 25°C, and a contact time of two hours. The findings, which are shown in the table below, provide insight into the ideal concentration of $mSiO_2$ needed for the effective removal of hazardous metal ions from water-based solutions by showing how the adsorption capacity and removal percentage change with increasing adsorbent dosage. Figure (10) shows that at every test temperatures, the ions Pb^{2+}, Cd^{2+}, and Cr^{3+} are efficiently adsorbed. The findings show that the mesoporous silica adsorbent ($mSiO_2$) removes metal ions more effectively when its mass increases. This is mainly because the corresponding increase in surface area creates more active adsorption sites. However, after a certain point, no discernible increase in removal efficiency was seen, even though the adsorbent dosage was changed from 0.01 to 0.05 g. Particle aggregation at higher adsorbent masses is probably the cause of this plateau effect, which can limit additional adsorption capacity by reducing the effective surface area and blocking available active sites as shown in table (5) and Fig. (10) [34].

4.5 Adsorption Isotherms

Using established adsorption isotherm models, the adsorption performance of mesoporous silica ($mSiO_2$) synthesized from natural sources is evaluated in this section. The study looked into how heavy metal ions are distributed between the liquid and solid phases through three widely applied isotherm models: Langmuir, Freundlich, and Temkin, based on experimental data [35]. These mathematical models, commonly referred to as adsorption isotherms, describe the capacity of an adsorbent to retain a particular substance on its surface under equilibrium conditions. Irving Langmuir [35] proposed the Langmuir isotherm, which is based on the assumption that monolayer adsorption occurs onto a homogeneous surface with a finite number of identical sites**.** This model is based on the premise that each active site on the adsorbent can accommodate one molecule, forming covalent, ionic, or coordination bonds, with minimal interaction between adsorbed species. The model also assumes that adsorption occurs at constant temperature and that every site has the same adsorption energy.

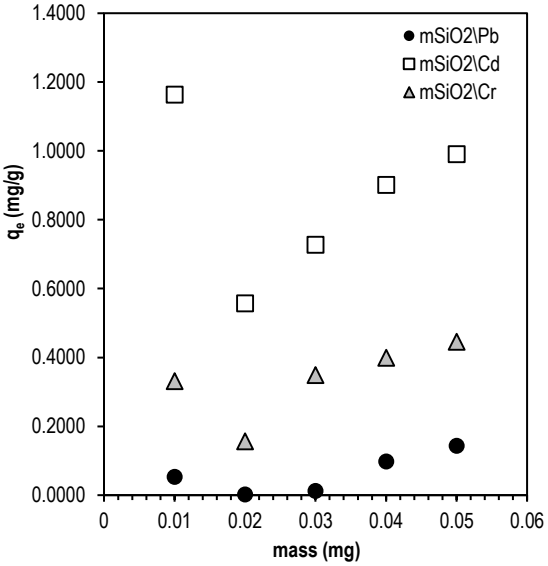

Fig. (10) Effect of adsorbent mass on capacity of Pb^{2+}, Cd^{2+}, and Cr^{3+} ions using mesoporous silica ($mSiO_2$)

It is possible to represent the Langmuir isotherm mathematically by the nonlinear Eq. (4) as follows, whereas equation (5) represents the linear formula for the Langmuir isotherm as follows:

$$q_e = \frac{q_{max} \cdot K_L \cdot C_e}{1 + K_L \cdot C_e} \quad (4)$$

$$\frac{C_e}{q_e} = \frac{1}{K_L \cdot q_{max}} + \frac{C_e}{q_{max}} \quad (5)$$

Where C_e is the adsorbate's equilibrium concentration in mg/L, q_e, at equilibrium, the amount adsorbed is expressed in mg/g, q_{max}, for a monolayer coverage, the maximum adsorption capacity is expressed in mg/g, K_L is the equilibrium constant correlated with the adsorption binding energy in (L/mg). For instance, the maximum adsorption capacities (q_e) of mesoporous silica ($mSiO_2$) for Pb^{2+}, Cd^{2+}, and Cr^{3+} were discovered to be, respectively, 43.67 mg/g, 40.65 mg/g, and 67.11 mg/g.

An empirical model for assessing adsorption processes on heterogeneous surfaces is provided by the Freundlich isotherm, particularly under conditions of low solute concentrations and constant temperature at equilibrium. Unlike the Freundlich model takes surface

adsorption into consideration, whereas the Langmuir model assumes monolayer adsorption on uniform surfaces, heterogeneity and variation in adsorption energy. Originally developed by Freundlich based on experimental observations [37], this model is particularly effective in describing multilayer adsorption behavior in systems involving complex surface interactions. The Freundlich isotherm can be expressed by a nonlinear equation

$$q_e = K_f . C_e^{\frac{1}{n}} \quad (6)$$

$$\mathrm{Ln}\, q_e = \mathrm{Ln}\, k_f + \frac{1}{n} \mathrm{Ln}\, C_e \quad (7)$$

while the nonlinear formula for the Freundlich isotherm is shown by Eq. (7), q_e is the amount adsorbed in mg/g at equilibrium, C_e is the adsorbate's equilibrium concentration in mg/litre

The distribution of adsorption bonds on the adsorbent surface is related to the Freundlich isotherm constants K_f and n, which depend on the adsorbent's nature and temperature, and the adsorbate. Freundlich isotherm constants, K_f and n, are connected to the adsorption intensity on the adsorbent surface as well as the distribution of adsorption sites. Temperature, the physicochemical characteristics of the adsorbent, and the type of adsorbate are some of the variables that affect these constants. In addition, Temkin proposed an adsorption isotherm model to describe the behavior of gas adsorption onto solid surfaces, which was later extended to liquid-phase systems. The Temkin isotherm takes into consideration the interactions between the adsorbent and the adsorbate, indicating that as coverage increases, the heat of adsorption falls linearly as opposed to exponentially. This model effectively represents systems in which adsorbate adsorbent interactions influence the energy distribution of adsorption sites. The Temkin isotherm can be represented using the following formulas [38]:

$$q_e = B_T \ln(A_t . C_e) \quad (8)$$

$$q_e = B_T \ln A_t + B_T \ln C_e \quad (9)$$

q_e is the quantity adsorbed at equilibrium in (mg/g), B_T is Temkin isotherm constant (J/mol), A_t is binding constant for Temkin isotherm equilibrium (L/g), C_e is the adsorbate's equilibrium concentration in mg/litre

The adsorption behavior of naturally synthesized mesoporous silica ($mSiO_2$) was evaluated using the interaction between the adsorbent and heavy metal ions under equilibrium conditions is described by adsorption isotherm models, such as Langmuir, Freundlich, and Temkin. In the Freundlich isotherm model, the adsorption capacity and intensity are denoted by the constants K_f and 1/n, respectively. The value of 1/n also indicates the degree of deviation from ideal linear adsorption. A lower 1/n value reflects stronger adsorption intensity and greater heterogeneity of the adsorbent surface. For mesoporous silica ($mSiO_2$), the maximum adsorption capacities (1/n) decreases, the q_m for Cd^{2+}, Pb^{2+}, and Cr^{3+} ions were discovered to be, respectively, 43.67 mg/g, 40.65 mg/g, and 67.11 mg/g. [39]. The Temkin isotherm, however, takes into consideration the impact of interactions between the adsorbent and the adsorbate. According to this model, as surface coverage increases, the heat of adsorption for every molecule in the adsorption layer falls linearly, reflecting energy variation across active binding sites. Unlike other models, the Temkin isotherm does not rely on extreme concentration assumptions at low or high limits. Based on this model, the B_T (J/mol) values, which correspond to the Temkin constant related to adsorption energy, were calculated to be 9.949, 7.3071, and 13.994 J/mol for Cd^{2+}, Pb^{2+}, and Cr^{3+} ions, respectively [40]. Langmuir constant provides its behavior with temperature change (describing the adsorption process's characteristics) and is reliant on Gibbs free energy of adsorption [41], Freundlich constant K_L, when increases. This suggests that the adsorption process is endothermic and chemical as the temperature rises. The fact that K_L decreases as temperature rises suggests that the adsorption process is endothermic and physical. This is consistent with the results obtained in our study. Temkin constant (B_T>0) indicates that the adsorption reaction of Cd^{2+}, Pb^{2+}, and Cr^{3+} ions is exothermic. From the R^2 values for all the studied isothermal models, it was concluded that the Cd^{2+}, Pb^{2+}, and Cr^{3+} ion adsorption in Temkin and Langmuir isotherm models consistent more than with Freundlich isothermal model. This conclusion was reached through the high R^2 value [41] as shown in table (2).

The latest Langmuir effect ($R^2 > 0.97$) indicates that the adsorption is monoclinic, with the highest q_m for chromium and the highest K_L for cadmium and lead, to what is clearer than Freundlich (1/n<1) but the adsorption at low points with high K_F for lead, and as a result the adsorption strength (B_T) decreases for the surface coverage with the highest K_T for lead. The adsorption behavior of Pb^{2+}, Cd^{2+}, and Cr^{3+} ions onto mesoporous silica ($mSiO_2$) at 25°C aligns most strongly with the Langmuir isotherm model, as evidenced by high R^2 values (0.9757–0.9926). This indicates that the adsorption process is primarily governed by monolayer coverage on a surface with homogeneous active sites and uniform adsorption energy. Specifically, Cr^{3+} showed the highest adsorption capacity (q_m= 67.11 mg/g) and strongest correlation ($R^2 = 0.9926$), reflecting a highly favourable monolayer adsorption interactions due to its trivalent nature. Cd^{2+} and Pb^{2+} also exhibited strong Langmuir behavior with q_m values of 43.67 mg/g and 40.65 mg/g, respectively. The Freundlich model showed lower R^2 values, especially for Pb^{2+} (0.9128), suggesting limited surface heterogeneity and indicating that multilayer adsorption was not dominant. Interestingly, the negative 1/n value for Cr^{3+} suggests limitations in applying the Freundlich model for this ion, reinforcing the suitability of the Langmuir approach. Temkin model fitting further supported the Langmuir

conclusions, with moderate adsorption energies (B_T values of 7.3-13.9 J/mol), indicating physicochemical adsorption with decreasing heat of adsorption as surface coverage increases.

4.6 Thermodynamic Analysis

Using the van't Hoff equation, thermodynamic parameters for the adsorption of toxic metal ions (Pb^{+2}, Cd^{2+}, and Cr^{3+}) onto mesoporous silica made from natural porcelanite rock were assessed. From this analysis, to learn more about the nature and spontaneity of the adsorption process, the standard enthalpy change (ΔH°) and entropy change (ΔS°) of adsorption were measured. These variables help elucidate the energy changes and degree of disorder associated with the interaction of the metal ions in aqueous solution with the adsorbent [42]

$$\mathrm{LnK} = \frac{\Delta S}{R} - \frac{\Delta H}{RT} \quad (10)$$

$$K = \frac{Q_e}{C_e} \quad (11)$$

where K is the equilibrium constant, R is the universal gas constant, and T is the absolute temperature

The standard enthalpy change (ΔH°) and standard entropy change (ΔS°) values were calculated by plotting 1/T against ln K. The slope and intercept of the resulting linear van't Hoff plot are pure. When Pb^{2+}, Cd^{2+}, and Cr^{3+} ions are adsorbed, the standard Gibbs free energy change (ΔG°) is then was calculated using the thermodynamic relation

$$\Delta G = \Delta H - T \times \Delta S \quad (12)$$

Thermodynamic results indicate that the adsorption of the three metal ions onto the mesoporous silica surface is spontaneous at the studied temperatures, as demonstrated by the negative values of the standard free energy (ΔG°). The value of ΔG° gradually decreases with increasing temperature, indicating an increase in the spontaneity of adsorption with increasing temperature. As for the enthalpy change (ΔH°), all values were negative (Pb^{2+}= -0.00399 kJ/mol, Cd^{2+}= -0.00774 kJ/mol, Cr^{3+}= -0.0070 kJ/mol), indicating that the adsorption process occurs exothermally, a typical feature of physical adsorption. The change in entropy (ΔS°) was positive for all elements, reflecting an increase in randomness at the interface between the surface and the solution during adsorption, which may be attributed to the release of water molecules associated with the ions during their fixation on the surface. The variation in values between the elements reflects the different nature of the interaction and adsorption behavior of each ion, with silica showing the highest efficiency towards chromium, followed by lead, then cadmium, in terms of ΔG° values as shown in table (3) [43].

4. Conclusions

In the Anbar Governorate, mesoporous silica ($mSiO_2$) was effectively utilized to extract lead (Pb^{2+}), cadmium (Cd^{2+}), and chromium (Cr^{3+}) ions from tainted water after it was successfully extracted from porcelanite rocks. For all ions, the results demonstrated high adsorption efficiencies of over 97%, with chromium The material's structural properties and adsorption-friendly surface were confirmed showing a notable advantage. Monolayer adsorption on a homogeneous surface was indicated by the adsorption models' improved fit to the Langmuir and Temkin models. The exothermic, spontaneous, and physical nature of the process was confirmed by the negative thermodynamic values (ΔH°, ΔG°, and ΔS°). These findings lend credence to the use of naturally occurring $mSiO_2$ as an economical and efficient material for heavy metal water treatment.

References

[1] A.K. Sahu et al., "Ecological and human health risk associated with heavy metals in sediments and bioaccumulation in some commercially important fishes in Mahanadi River, Odisha, India", *Environ. Chem. Ecotoxicol.*, 5 (2023) 168-177.

[2] A. Achkir et al., "Implication of sewage sludge increased application rates on soil fertility and heavy metals contamination risk", *Emerg. Contam.*, 9(1) (2023) 100200.

[3] A.E. Gahrouei et al., "From classic to cutting-edge solutions: A comprehensive review of materials and methods for heavy metal removal from water environments", *Desalin. Water Treat.*, 319 (2024) 100446.

[4] W.M. Saod et al., "Water quality index along the Euphrates between the cities of Al-Qaim and Falluja: A comparative study", *IOP Conf. Ser. Earth Enviro. Sci.*, 779 (2021) 012058.

[5] J. Briffa, E. Sinagra and R. Blundell, "Heavy metal pollution in the environment and their toxicological effects on humans", *Heliyon*, 6(9) (2020) e04691.

[6] M.M. Dehkordi et al., "Soil, air, and water pollution from mining and industrial activities: sources of pollution, environmental impacts, and prevention and control methods", *Results Eng.*, 23 (2024) 102729.

[7] N. Luo, "Methods for controlling heavy metals in environmental soils based on artificial neural networks", *Sci. Rep.*, 14(1) (2024) doi: 10.1038/s41598-024-52869-9.

[8] S. Mitra et al., "Impact of heavy metals on the environment and human health: Novel therapeutic insights to counter the toxicity", *J. King Saud Univ. - Sci.*, 34(3) (2022) 101865.

[9] F. Guerra et al., "Heavy metals in vegetables and potential risk for human health," *Sci. Agric.*, 69(1) (2012) 54-60.

[10] K. Nomiyama et al., "Lead induced increase of blood pressure in female lead workers," *Occup. Environ. Med.*, 59(11) (2002) 734-738.

[11] Y. Arul et al., "Enhanced removal of Pb^{+2} (II) and Cd (II) ions from aqueous systems using coated magnetic nanoparticles in activated carbon derived from corncob waste", *Surf. Interfaces*, 40 (2023) 103095.
[12] D. Singh, "Activated carbon nanoparticles generated from coffee husk: A pioneering biomaterial for improving drug targeting in cancer", *Nano-Struct. Nano-Objects*, 38 (2024) 101134.
[13] G. Li et al., "Activated carbons with extremely high surface area produced from cones, bark and wood using the same procedure", *RSC Adv.*, 13(21) (2023) 14543-14553.
[14] L. Coudert et al., "Remediation processes for wood treated with organic and/or inorganic preservatives," in **Handbook of Recycled Concrete and Demolition Waste**, Elsevier (2013), pp. 526-554.
[15] S.R. Dhokpande et al., "A review outlook on methods for removal of heavy metal ions from wastewater", *Sep. Purif. Technol.*, 350 (2024) 127868.
[16] B. Janković et al., "Physico-chemical characterization of carbonized apricot kernel shell as precursor for activated carbon preparation in clean technology utilization", *J. Clean. Prod.*, 236 (2019) 117614.
[17] I.A. Mawlood et al., "Characterization and use of activated carbon synthesized from sunflower seed shell in the removal of Pb^{+2}(II), Cd(II), and Cr(III) ions from aqueous solution", *Environ. Monit. Assess.*, 196(4) (2024) 364.
[18] I.I. Gurten et al., "Preparation and characterisation of activated carbon from waste tea using K_2CO_3", *Biomass Bioenergy*, 37 (2012) 73-81.
[19] M. Issaoui et al., "Palm wastes valorization for wastewaters treatment," in **Palm Trees and Fruits Residues: Recent Advances for Integrated and Sustainable Management**, Academic Press (2022), pp. 243-308.
[20] M. Abu Taleb et al., "Hybrid bioadsorbents for heavy metal decontamination from wastewater: A review", *Int. J. Mater. Technol. Innov.*, 2(1) (2022) 5-19.
[21] R. Ganjoo et al., "Activated Carbon: Fundamentals, Classification, and Properties", *Act. Carbon*, 5 (2023) 1-22.
[22] M. Gayathiri et al., "Activated carbon from biomass waste precursors: Factors affecting production and adsorption mechanism", *Chemosphere*, 294 (2022) 133764.
[23] J. R. Bastidas-Oyanedel and J. E. Schmidt, "Waste biorefinery in arid/semiarid regions", in **Waste Biorefinery: Potential and Perspectives**, Elsevier (2018), pp. 605-621.
[24] L. Luo et al., "Synthesis of activated carbon from biowaste of fir bark for methylene blue removal", *Royal Soc. Open Sci.*, 6(9) (2019) 190523.
[25] A. Al-Ani, C. Freitas and V. Zholobenko, "Nanostructured large-pore zeolite: The enhanced accessibility of active sites and its effect on the catalytic performance", *Micropor. Mesopor. Mater.*, 293 (2020) 109805.
[26] M.I. Al Biajawi et al., "Investigation the effect of nanocarbon tube prepared from tea waste on microstructure and properties of cement mortar", *Environ. Sci. Pollut. Res.*, 32 (2023) 13106-13119.
[27] D.A. Ghafoor, W.M. Saod and N. Mohammed, "Green synthesis of gold nanoparticles using pineapple extract and study their analytical characterization and antibacterial activity", *Syst. Rev. Pharm.*, 11(2) (2020) 462-465.
[28] W.M. Soad et al., "Novel economical adsorbents employed as stationary phases in column chromatography for pollution removal", *Microchem. J.*, 2016 (2025) 114636.
[29] W.M. Saod et al., "Zinc oxide–mesoporous silica nanocomposite: preparation, characterisation and application in water treatment for lead, cadmium and chromium removal", *Int. J. Environ. Anal. Chem.*, 104(20) (2023) 9772-9784.
[30] V.K. Pecharsky and P.Y. Zavalij, **"Fundamentals of Powder Diffraction and Structural Characterization of Materials"**, Springer (2009).
[31] R. Ben Brahim and A. Chehaidar, "Small-Angle X-Ray Scattering of Amorphous Germanium: Numerical Modeling", *Adv. Mater. Phys. Chem.*, 3(1) (2013) 19-30.
[32] R.M. Silverstein and F.X. Webster, **"Spectrometric Identification Of Organic Compounds"**, 6th ed., Wiley (1996).
[33] H. Rustamaji et al., "Modification of hydrochar derived from palm waste with thiourea to produce N, S co-doped activated carbon for supercapacitor", *Sustain. Chem. Environ.*, 7 (2024) 100132.
[34] D.B. Williams and C.B. Carter, "Transmission Electron Microscopy", in **A Textbook for Materials Science**, 2nd ed., Springer (NY, 2009), pp. 1-757.
[35] L. Reimer, **"Scanning Electron Microscopy: Physics of Image Formation and Microanalysis"**, Springer (Berlin, 1998).
[36] W. Plazinski, "Equilibrium and kinetic modeling of metal ion biosorption: On the ways of model generalization for the case of multicomponent systems", *Adsorption*, 19(2-4) (2013) 659-666.
[37] K.Y. Foo and B.H. Hameed, "Insights into the Modeling of Adsorption Isotherm Systems", *Chem. Eng. J.*, 156(1) (2009) 2-10.
[38] W.M. Saod et al., "Study of effective removal of nickel and cobalt from aqueous solutions by

FeO@mSiO$_2$ nanocomposite", *Results Chem.*, 13 (2025) 101992.
[39] W. Plazinski, W. Rudzinski and A. Plazinska, "Theoretical Models of Sorption Kinetics Including a Surface Reaction Mechanism: A Review", *Adv. Colloid Interface Sci.*, 152(1-2) (2009) 2-13.
[40] T.A Saleh, "Isotherm, kinetic and thermodynamic studies on Hg(II) adsorption from aqueous solution by silica–multiwall carbon nanotube composite", *J. Mol. Liquids*, 307 (2020) 112934.
[41] A.A. Al-Saadi and T.S. Jamil, "Mesoporous silica-based adsorbents for the removal of heavy metal ions from wastewater: A review", *Environ. Nanotech. Monitor. Manage.*, 16 (2021) 100515.
[42] M.A. Rahman, M.R. Islam and M. Shahruzzaman, "Thermodynamic insight into adsorption of Pb(II), Cd(II), and Cr(III) using biosilica nanoparticles", *Environ. Res.*, 212 (2022) 113148.
[43] M.I. Khan et al., "Utilization of natural and modified mesoporous silica for remediation of toxic metal ions from aqueous media: Mechanistic and thermodynamic perspectives", *J. Environ. Chem. Eng.*, 11(1) (2023) 109215.

Table (2) Effect of pH on Pb^{2+}, Cd^{2+} and Cr^{3+} capacity and removal, with initial solution concentration 30 mg/L, 0.01 mg sorbent and 2 h equilibration time (using ($mSiO_2$)

pH	Ce.(mg/L) Pb	qe.(mg/g)	%R	Ce.(mg/L) Cd	qe.(mg/g)	%R	Ce. (mg/L) Cr	qe.(mg/g)	%R
pH2	6.76	23.24	3.86	83.33	26.14	87.12	5.00	25.00	83.32
pH3	1.49	28.51	2.09	87.42	27.91	93.04	3.77	26.23	87.41
pH4	0.67	29.33	1.36	91.34	28.64	95.47	2.60	27.40	91.95
pH5	0.60	29.41	1.20	95.68	28.80	96.00	1.30	28.70	95.67
pH6	0.40	29.60	1.08	97.19	28.92	96.41	0.84	29.16	97.18
pH7	0.12	29.88	0.52	99.37	29.48	98.27	0.19	29.81	99.36
pH8	0.01	29.99	0.45	99.51	29.55	98.50	0.15	29.85	99.50

Table (4) Initial concentration effect of on Pb^{2+}, Cd^{2+} and Cr^{3+} capacity and removal, with initial solution concentration (10-50 ml) mg/L, 0.01 mg sorbent and 2 h equilibration time (using ($mSiO_2$)

Concentration (mg/L)	Ce (mg/L) Pb	q_e (mg/g)	%R	Ce (mg/L) Cd	q_e (mg/g)	%R	Ce (mg/L) Cr	q_e (mg/g)	%R
10	0.006	9.993	99.93	0.037	9.963	99.6300	0.096	9.903	99.03
20	0.015	19.984	99.92	0.097	19.902	99.5108	0.260	19.740	98.70
30	0.304	29.696	98.98	0.565	29.434	98.1153	0.496	29.503	98.34
40	0.466	39.530	98.83	0.937	39.06	97.6575	0.723	39.276	98.19
50	0.735	49.264	98.52	1.4034	48.59	97.1931	0.934	49.065	98.13

Table (3) Effect of contact duration on Pb^{2+}, Cd^{2+} and Cr^{3+} capacity and removal, with initial solution concentration 30 mg/L, 0.01 mg sorbent and 2 h equilibration time using $mSiO_2$

Time	Ce (mg/L) Pb	q_e (mg/g)	%R	Ce (mg/L) Cd	q_e (mg/g)	%R	Ce (mg/L) Cr	q_e (mg/g)	%R
T10	0.81	29.18	97.12	1.47	28.52	95.07	0.86	29.13	97.12
T20	0.46	29.53	98.45	1.37	28.63	95.41	0.45	29.53	98.45
T35	0.32	29.67	98.55	1.28	28.72	95.75	0.43	29.56	98.55
T45	0.15	29.84	98.77	1.00	28.99	96.63	0.37	29.63	98.77
T60	0.08	29.91	99.33	0.98	29.01	96.71	0.20	29.79	99.33
T90	0.06	29.93	99.59	0.77	29.22	97.43	0.12	29.87	99.59
T120	0.05	29.94	99.64	0.73	29.26	97.56	0.10	29.89	99.64

Table (5) Effect of adsorbent mass on Pb^{2+}, Cd^{2+} and Cr^{3+} capacity and removal, with initial solution concentration 30 mg/L, (0.01-0.05 mg) sorbent and 2 h equilibration time using $mSiO_2$

Mass (mg)	Ce (mg/L) Pb	q_e (mg/g)	%R	Ce (mg/L) Cd	q_e (mg/g)	%R	Ce (mg/L) Cr	q_e (mg/g)	%R
0.01	0.0536	29.99	99.82	1.1639	28.83	96.12	0.3320	29.66	98.89
0.02	0.0023	14.99	99.99	0.5575	14.72	98.14	0.1566	14.92	99.47
0.03	0.0127	9.99	99.95	0.7282	9.75	97.57	0.3495	9.88	98.83
0.04	0.0985	7.49	99.67	0.9014	7.27	96.99	0.3995	7.40	98.66
0.05	0.1435	5.990	99.52	0.9907	5.80	96.69	0.4460	5.91	98.51

Table (6) All adsorption isotherm model values (Freundlich, Langmuir, and Temkin)

Langmuir	Line equation	R^2	q_m (mg/g)	K_L (L/mg)
Pb-$mSiO_2$ (25°C)	0.0004x + 0.0246	0.9757	40.65040	10162.612
Cd-$mSiO_2$ (25°C)	0.0029x + 0.0229	0.986	43.66812	15057.971
Cr-$mSiO_2$ (25°C)	0.0084x + 0.0149	0.9926	67.11409	7989.773
Freundlich	**Line equation**	**R^2**	**1/n**	**K_F**
Pb-$mSiO_2$ (25°C)	0.2752x + 1.6892	0.9128	0.2752	48.88774
Cd-$mSiO_2$ (25°C)	0393x +1.6109	0.9593	0.393	40.82254
Cr-$mSiO_2$ (25°C)	0.0808x + 0.0127	0.9615	0.0808	1.029675
Temkin	**Line equation**	**R^2**	**B_T (J/mol)**	**K_T (L/mg)**
Pb-$mSiO_2$ (25°C)	7.3071x + 48.665	0.9724	7.3071	780.5204
Cd-$mSiO_2$ (25°C)	9.9493x +42.679	0.9834	9.9493	72.94083
Cr-$mSiO_2$ (25°C)	13.994x + 41.092	0.9595	13.994	18.8479

Table (7) Thermodynamic parameters for Pb^{2+}, Cd^{2+}, and Cr^{3+} ions adsorption on $mSiO_2$ at pH=7

Adsorbents	C_0 (mg/L)	C_e (mg\L)	T (K)	K_L	ΔG° (kJ/mol)	ΔH° (kJ/mol)	ΔS° (J/K.mol)	R^2
Pb-$mSiO_2$ (25°C)	30	0.4823	308	61.500	-10.548	-0.00399	21.30961	0.988
Pb-$mSiO_2$ (25°C)	30	0.4993	318	59.081	-10.784			
Pb-$mSiO_2$ (25°C)	30	0.52712	328	55.913	-10.973			
Cd-$mSiO_2$ (25°C)	30	0.612	308	48.02	-9.91	-0.00774	7.063574	0.999
Cd-$mSiO_2$ (25°C)	30	0.6696	318	43.80	-9.99			
Cd-$mSiO_2$ (25°C)	30	0.7329	328	39.93	-10.05			
Cr-$mSiO_2$ (25°C)	30	0.5204	308	56.648	-10.337	-0.0070	10.65023	0.991
Cr-$mSiO_2$ (25°C)	30	0.5594	318	52.623	-10.478			
Cr-$mSiO_2$ (25°C)	30	0.6141	328	47.860	-10.539			

